

UDC 669.017:669.715:669.018.25:669.056.91

WEAR RESISTANCE OF ALUMINUM ALLOY A356 AFTER THOROUGH ANODIC OXIDATION

Aziz Bariş Başıyigit,¹ Zeki Azakli,² Recep Gümrük,³ and Osman Bican¹

Translated from *Metallovedenie i Termicheskaya Obrabotka Metallov*, No. 6, pp. 58 – 64, June, 2023.

Original article submitted January 3, 2022.

The efficiency of thorough anodic oxidation of ASTM A356 aluminum alloy as an alternative to painting its surface is studied. Microstructure, phase composition, and microhardness of oxidized layers of various thicknesses (45, 65, 80 and 90 μm) are determined. Solid particle erosion tests are conducted in accordance with ASTM G76 and MIL STD 3033. It is established that with an increase in oxidized layer thickness aluminum alloy wear resistance is reduced and the surface roughness is reduced.

Key words: aluminum alloy A356, hard anodic oxidation, microstructure, phase composition, wear resistance, roughness.

INTRODUCTION

Aluminum alloy A356 (Russian analog AK7) is related to structural thermally strengthened silumins and it is used extensively in the aviation and automobile industries. The alloy has a combination of good casting properties with satisfactory mechanical characteristics in a thermally strengthened condition, i.e., after quenching and ageing [1 – 3]. Alloy A356 is also subjected to surface treatment by coating application, anodic oxidation, and surface strengthening. Thorough anodic oxidation is normally conducted within baths with sulfuric acid with formation of a surface layer 5 – 18 μm thick, which considerably improves alloy wear resistance. However, a high silicon content up to 7.5 wt.% reduces oxidation efficiency [1, 2, 4] and requires stringent control of current density, process duration and electrolyte temperature [5], and also metal surface roughness [6]. Without observation of these manufacturing parameters quality of the oxide layer formed is reduced and cracks may form within it [4, 7].

During oxidation at an aluminium alloy surface an oxide film forms consisting of two layers, i.e., porous and dense (compact). The dense layer is a thin barrier, and the porous layer is densely packed spherical cells. Thorough anodic oxidation increases the rate of compact layer film formation [8, 9]. In this case the most important process parameters are the anodizing voltage [10] and anodic oxidation bath composition [11]. New methods have also been developed for anodizing without using an electric current [12]. A method of hybrid pulse anodizing provides more uniform pore distribution within an oxide layer [13]. Chemical composition and impurity content have an effect on oxide film formation on aluminium alloys [14 – 17]. It should be noted that there are quite a number of publications devoted to studying aluminium alloy hard anodic oxidation efficiency, but selective study of alloy A356 is not currently known.

The aim of the present work is a study of the microstructure, mechanical, and tribological properties of aluminium alloy A356 after thorough anodic oxidation using as an alternative to the traditional method galvanic coating and coloring during wheel disk production.

METHODS OF STUDY

Industrial alloy ASTM A356 (ISO; AlSi7Mg) was used for the study. An optico-spectral analysis method in an Amatex Spectromax spectrometer established that it has the following chemical composition, wt.%: 92.00 Al, 7.070 Si,

¹ Faculty of Engineering, Department of Metallurgical and Materials Engineering, Kirikkale University, Kirikkale, Turkey (e-mail: abbasyigit@kku.edu.tr, bican@kku.edu.tr).

² Faculty of Engineering, Department of Mechanical Engineering, Gümüşhane University, Gümüşhane, Turkey (e-mail: zekiazakli@gumushane.edu.tr).

³ Faculty of Engineering, Department of Mechanical Engineering, Karadeniz Technical University, Turkey (e-mail: rgumruk@ktu.edu.tr).

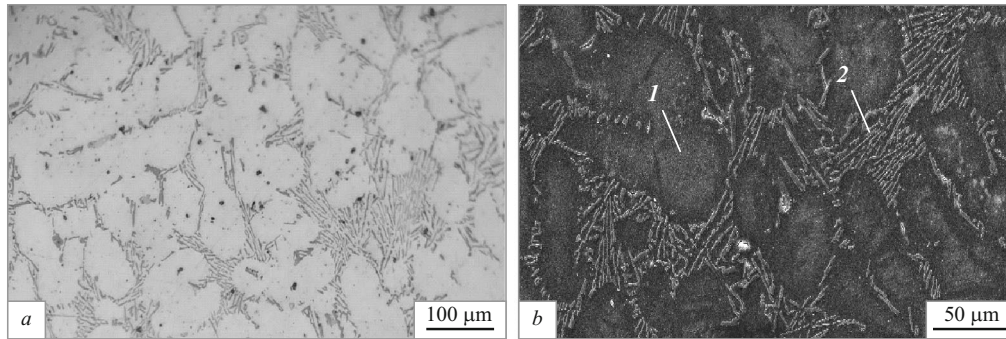


Fig. 1. Alloy A356 microstructure in original condition: *a*) light microscope; *b*) electron microscope; 1) α -solid solution based upon Al (Aluminum rich α -phase); 2) α + Si eutectic (Hypoeutectic Silicon).

0.255 Mg, 0.182 Fe, 0.116 Ti, 0.038 Zn, 0.007 Mn, 0.005 Cu, 0.002 Ni, 0.001 Cr, < 0.001 Sn, 0.323, residual impurities.

From the original cast workpieces 14 experimental specimens were prepared with a size of $4 \times 20 \times 20$ mm. Thorough anodic oxidation was performed in a bath with 19% sulfuric acid with a constant current density of 2 A/dm^{-2} , voltage 19 V, and working temperature 2°C . Specimens were cleaned with caustic soda after sand blasting treatment and immersion in a bath with sulfuric acid for different immersion times: 40, 60, 80, and 90 min. after oxidation at an alloy surface there was formation of a layer of different average thickness of 45, 65, 80, and 90 μm .

Microstructural studies were performed using a Leica Brand Metallurgical microscope after grinding with emery paper with a grain size of 240 to 800 μm and polishing with 6 μm diamond paste. Metallographic specimens were etched in $\text{HF} + \text{HCl} + \text{HNO}_3$ for 15 sec by immersion [18]. Studies by means of a scanning electron microscope (SEM) were performed in a Jeol JSM-5600 instrument.

X-ray structural studies were accomplished in an Ultima-IV Rigaku diffractometer with copper radiation at 40 kV, 30 mA, with a scanning rate of 2 deg/min, pitch 0.02° with scanning range $10 - 90^\circ$.

Specimen microhardness ($HV_{0.1}$) was determined in a Vickers Emcotest Durascan 20 hardness meter at 22°C and a load of 100 g. oxide layer thickness was evaluated from results of studying the microstructure and also according to the different microhardness of the alloy surface layer and core [19 – 22].

Alloy wear resistance was determined with erosion testing by solid particles in accordance with the ASTM G76 and MIL STD 3033 standard [23, 24]. Alloy test specimens were installed within a test system and subjected to erosion by solid aluminium oxide particles with a nominal size of 50 μm supplied at a rate of 2.5 g/min by compressed air through a nozzle 2 mm in diameter. Testing was conducted with particle impact angles of 30, 45, 60, and 90° and impact speed 74 m/sec. Erosion particle flow rate was measured by a double disc method [25]. Particle impact rate of 74 m/sec was implemented by application of pressure 300 mbar.

Specimen weight loss was measured after each 2 min of testing using a precision balance with accuracy of 0.1 mg. The overall erosion test duration was 8 min. The erosion agent (abrasive dust) used was aluminium oxide (Al_2O_3) powder with an average particle size of 50 μm . Powder was fed to a test specimen surface at a rate of 2.5 g/min.

After erosion testing with hard particles specimen surface roughness was determined in accordance with standards EN ISO 16610, EN 10049 and EN ISO 4287 [26 – 28] in a Nanofocus μscan -custom 3d profilometer.

RESULTS AND DISCUSSION

Aluminium alloy A356 in the original condition (before anodizing) has a typical hypoeutectic silumin structure [18] consisting of α -solid solution and eutectic with acicular morphology silicon inclusions (Fig. 1).

The alloy A356 microstructure (SEM) after thorough anodic oxidation with an oxide layer of different thickness is shown in Fig. 2. An anodically-oxidized layer is clearly seen within the structure of all alloy specimens after treatment, and the layer thickness for different specimens after the same oxidation regime hardly differs. However, in some specimens subsurface microcracks were observed (Fig. 2c and d). This defect may arise after thorough anodizing since the layer formed at a surface is very hard and brittle [4]. Cracks are observed within both thick and thin layers, but with an increase in oxide layer thickness their amount increases. X-ray structural analysis showed that the oxide layer consists mainly of Al_2O_3 oxide (Fig. 3). In addition, within a diffraction pattern reflections are also seen from α -phase rich in aluminium (111), (222), (311) designated as A1.

Results of determining the layer thickness by a Vickers method are provided in Table 1. All specimens after the treatment test regimes may be separated with respect to oxide layer thickness δ_{la} into four groups: 1 — $\delta_{\text{la}} = 30 - 40 \mu\text{m}$; 2 — $\delta_{\text{la}} = 60 - 65 \mu\text{m}$; 3 — $\delta_{\text{la}} = 75 - 80 \mu\text{m}$; 4 — $\delta_{\text{la}} = 90 - 100 \mu\text{m}$. An increase in layer thickness leads to an insignificant increase in maximum microhardness value at a specimen surface. The average microhardness value for an

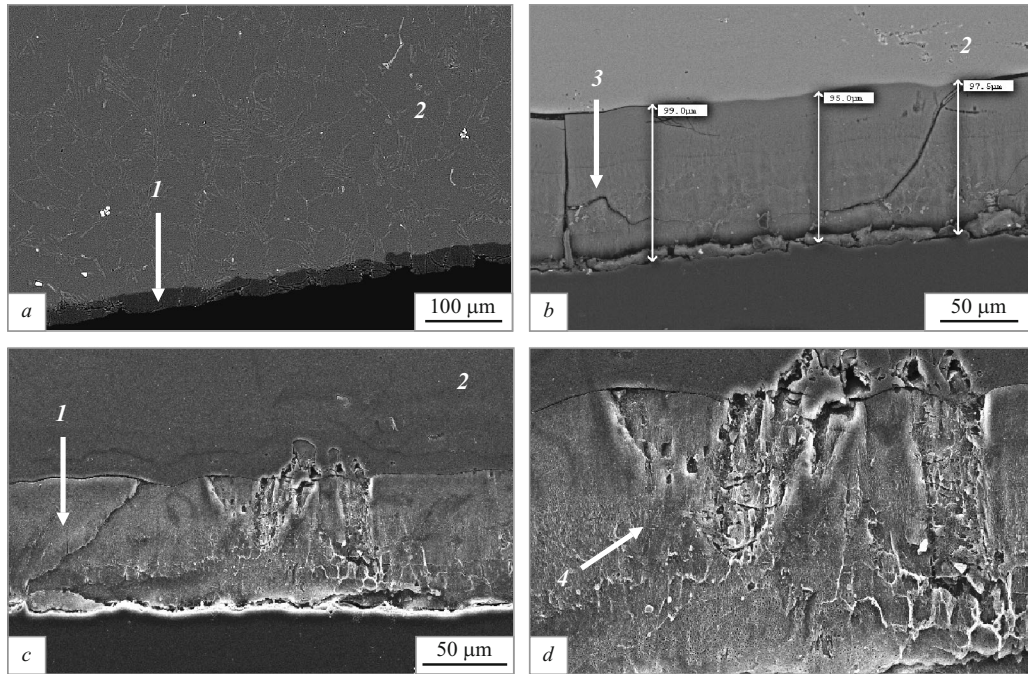


Fig. 2. Microstructure (SEM) of alloy A356 after anodic oxidation: *a*) oxide layer thickness 40; *b*) 90 – 100 μm; *c, d*) 75 – 80 μm; 1) hard anodic oxidation layer; 2) basic metal; 3) sub-surface microcracks; 4) sub-surface microcrack zone.

oxidized specimen surface of groups 1 and 2 is 370 HV, group 3 — 374 HV, and group 4 — 381 HV. The aluminium alloy specimen core hardness is 60 HV.

Test results are provided in Fig. 4 for the wear resistance of alloy A356 in the original condition and after oxidation by different regimes. It is seen that the best wear resistance applies to alloy A356 after oxidation. Therefore, an anodized surface coating reduces wear resistance of an aluminium alloy and weight loss during wear under action of hard particles increases linearly in all cases with an increase in test duration. Alloy erosion resistance also decreases with an in-

crease in oxide layer thickness. These data agree with results evaluating the structure (Fig. 2) and microhardness (Fig. 3) of alloy in different conditions. Comparative analysis showed that the amount of surface cracks and microhardness of an oxide layer increase with an increase in thickness, which points to an increase in coating brittleness.

Impact angle is an important parameter affecting the nature of material erosion behaviour. Depending upon impact angle material may develop both ductile and also brittle erosion behaviour [29]. Losses during ductile erosion are at a

TABLE 1. Microhardness $HV_{0.1}$ of Aluminum Alloy A3176 with Oxidized Layer of Different Thickness (δ_{la})

Specimen group	$\delta_{la}, \mu\text{m}$	$HV_{0.1}, \text{kgf/mm}^2$		Change in $HV_{0.1}$ through oxidized layer thickness*
		surface	core	
1	30 – 40	370	60	370 → 229 $HV_{0.1}$ (0 – 45 μm)
2	60 – 65	370	62	371 → 226 $HV_{0.1}$ (0 – 65 μm)
3	75 – 80	374	61	376 → 260 $HV_{0.1}$ (0 – 80 μm)
4	90 – 100	381	61	383 → 265 $HV_{0.1}$ (0 – 90 μm)

* Given in brackets is distance from the surface at which microhardness was measured.

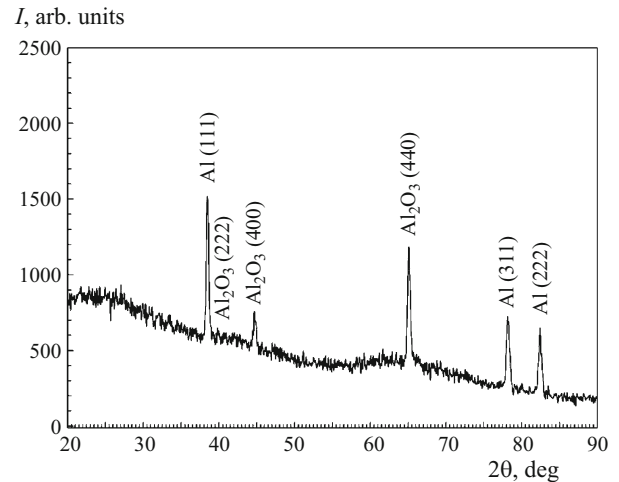


Fig. 3. Alloy A356 surface layer diffraction pattern after anodic oxidation.

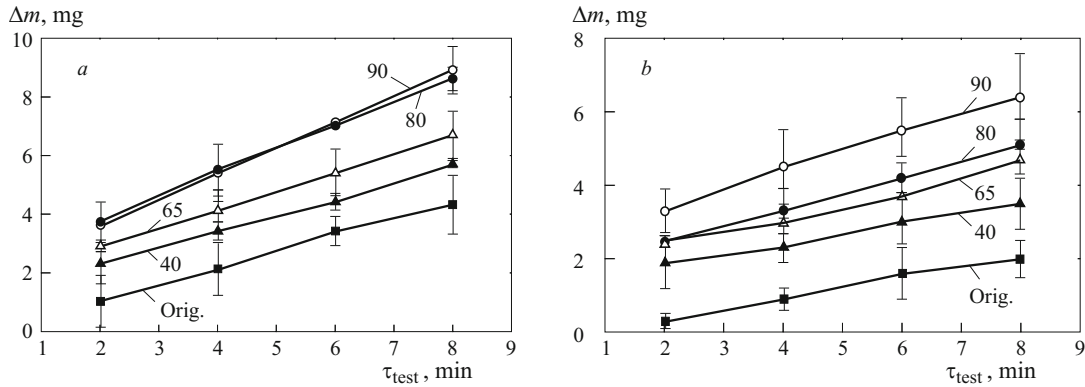


Fig. 4. Dependence of weight loss (Δm) of alloy A356 oxidized specimens during testing (τ_{test}) on erosion under action of solid particles with impact velocity 74 m/sec at angle 30° (a) and 90° (b): figures on curves are oxidized specimen thickness, μm ; Orig. is original condition without oxidation; Uncoated).

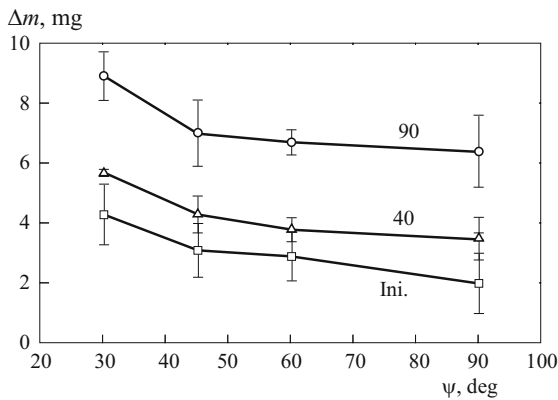


Fig. 5. Dependence of weight loss (Δm) of oxidized alloy A356 specimens on solid particle impact angle with velocity 74 m/sec during erosion testing: numbers on curves are oxidized specimen thickness, μm ; Orig. is original condition.

maximum with low impact angles and at a minimum with large angles, and with brittle behaviour erosion reaches maximum values with large impact angles. The effect of impact angle on the magnitude of alloys A356 erosion without oxidation and also with an oxide layer 40 and 90 μm thick is shown in Fig. 5. It is seen that for both particle impact angles erosion losses are greater for specimens with the greater oxide layer thickness. It may be suggested that losses increase in proportion with an increase in layer thickness. In addition,

TABLE 2. Surface Roughness (Ra) of Alloy A356 Specimens after Erosion Wear Testing

Condition	δ_{ia} ,* μm	Ra , μm
After oxidation	90	2.744
	40	3.079
Without oxidation	0	5.884

* Oxide layer thickness.

test results showed that with an increase in particle impact angle specimen weight loss decreases, which points to the more ductile erosion behavior of the alloy

Shown in Fig. 6 is the effect of particle impact angle on a two-dimensional wear profile for alloy A356 specimens in an original condition and after oxidation to a depth of 45 and 90 μm . Analysis of erosion craters at an alloy surface shows that the slope of pit walls in the form of a truncated cone decreases with an increase in layer thickness, and pit depth increases. This points to a change in alloy surface mechanical wear mechanisms with an increase in coating thickness.

Three-dimensional images of a wear surface after erosion testing of aluminium alloy in the test condition are provided in Fig. 7. It is seen that the specimen wear profile is generated in the form of pits having the shape of a truncated cone. Comparison of here-dimensional alloy wear profiles in different conditions confirm that the wall angle of inclination of a cone into the depth of a surface decreases with an increase in oxidized layer thickness, i.e., the diameter of the inlet part of erosion cone is greater the larger the layer thickness.

The results obtained agree with data in [30] where it was established that aluminum alloy 6061 wear resistance decreases after anodic oxidation of the surface. In [31] it has been demonstrated that an increase in oxide layer thickness on alloy 6061 reduces its wear resistance.

A study of wear surface roughness of specimens showed that it decreases with an increase in coating thickness, i.e., there is an increase in surface quality (Table 2). This regularity is probably explained by the corresponding increase alloy surface hardness since abrasive particles stick more readily to a soft surface. This indicates that the alloy surface wear mechanism changes with an increase in oxide layer thickness. Presence of abrasive particles during wear of ductile alloy without oxidation leads to an increase in its surface roughness. On alloy with an oxidized brittle layer particles wear a specimen surface, which leads to a reduction in surface roughness analogous to a grinding process.

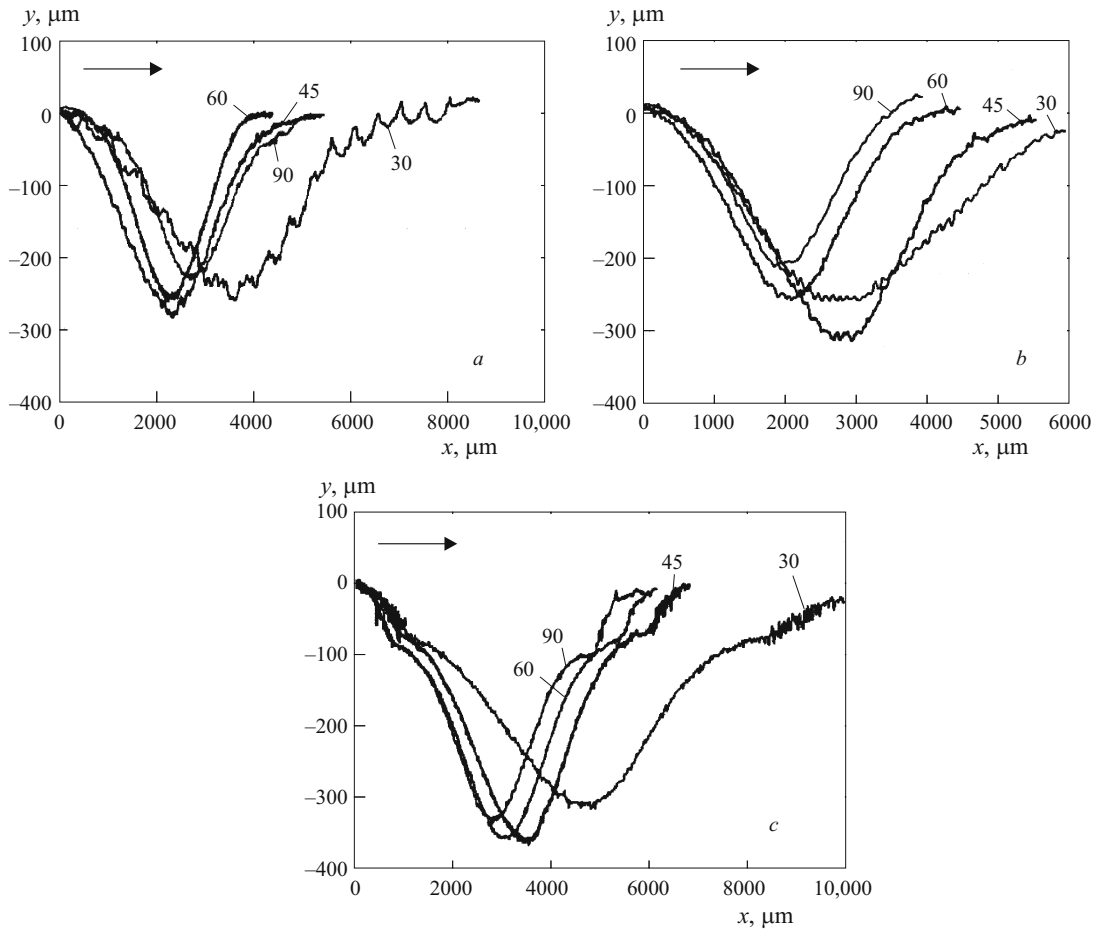


Fig. 6. Two-dimensional profile of erosion craters (y is depth, x is width) in alloy A356 surface in original condition (a) and after oxidation to a depth of 45 μm (b) and 90 μm (c) with erosion resting with hard particles (numbers on curves in degrees) (arrows show particle impact direction).

CONCLUSIONS

1. The microstructure, microhardness and tribological properties of aluminum alloy A356 after thorough anodic oxidation of different duration in a bath with 19% sulfuric acid with a direct current density of 2 A/dm^{-2} , voltage 19 V, and working temperature 2°C have been studied.

2. Aluminum alloy A356 microstructure in the original condition (before anodizing) consists of α -solid solution and eutectic with silicon acicular morphology.

3. An increase in oxidation duration from 40 to 90 min leads to an increase in surface oxide layer Al_2O_3 thickness from 45 to 90 μm .

4. With an increase in oxide layer thickness alloy wear resistance during erosion by solid particles with a different impact angles decreases as a result of an increase in the amount of surface microcracks and deterioration of oxide layer adhesion with aluminum.

5. With an increase in particle impact angle during erosion tests specimen weight loss decreases, which points to the more ductile erosion behaviour of the aluminum alloy.

After oxidation the greatest erosion resistance applies to alloy with the minimum oxide layer thickness equal to 40 μm . With an increase in oxide layer thickness alloy surface hardness increases, the roughness value is reduced, and surface quality after wear increases.

6. Alloy resistance to erosive wear is reduced with an increase in surface hardness as a result of an increase in oxide layer thickness. This indicates that the alloy A356 wear mechanism without oxidation has an aggregative nature both to sticking of particles to a surface and also shear of aluminum surface layers. After oxidation the alloy wear mechanism is abrasive in nature realized due to cutting.

Authors express their respects to Mechanical and Chemical Industries Corporation Armament Factory Heat and Surface Treatment Department Staff especially Mr. Mehmet Kalkan for precious laboratory supports.

REFERENCES

1. ASTM B26/B26 M-18E1. Standard Specification for Aluminum-Alloy Sand Castings, ASTM International (2018).

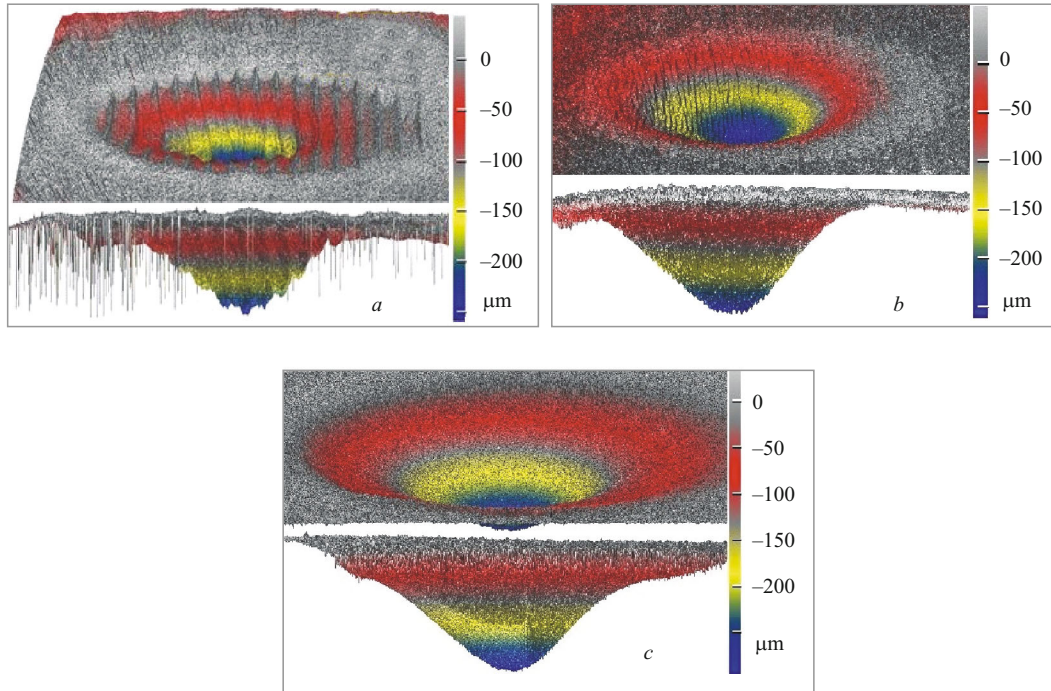


Fig. 7. Three-dimensional image of a surface and spectra for wear depth after alloy A356 erosion testing in the original condition (a) and after oxidation to a depth of 40 μm (b).

2. *BS EN 1706 Standard. Aluminum and Aluminum Alloy Castings Chemical Composition and Mechanical Properties* (2010).
3. *ASM Handbook Volume 2. Properties and Selection; Non-Ferrous Alloys and Special Purpose Materials*, ASM International (1990).
4. *ASM Handbook Committee, Surface Engineering, ASM Handbook Volume 5*, Electronic version, ASM International (1994).
5. A. Torrescano, M. Jeanette, M. Curioni, et al., "Effect of anodizing conditions on the cell morphology of anodic films on AA2024-T3 alloy," *Surf. Interface Anal.*, **51**(12), 1135 – 1143 (2019).
6. L. Lai, Y. Sun, H. Wu, et al., "Enhanced adhesive strength between SU-8 photoresist and titanium substrate by an improved anodic oxidation method for high aspect-ratio microstructures," *J. Micromech. Microeng.*, **29**(4), 1 – 10 (2019).
7. R. Sola, L. Tonelli, P. Shashkov, et al., "Anodizing of AA6082-T5 by conventional and innovative treatments: microstructural characterization and dry sliding behaviour," *Wear*, **458 – 459**, 203423 (2020).
8. L. Shaohua and J. Wang, "The technical support of nanoart: anodization process," *Anti-Corrosion Method. M.*, **66**(2), 242 – 250 (2019).
9. Z. Sarajan, "Preparation of A356 foam aluminum by means of titanium hydride," *Met. Sci. Heat Treat.*, **59**, 352 – 356 (2017).
10. E. O. Gordeeva, I. V. Roslyakov, A. I. Sadykov, et al., "Formation efficiency of porous oxide films in aluminum anodizing," *Russ. J. Electrochem.*, **54**(11), 990 – 998 (2018).
11. D. Elabar, T. Hashimoto, J. Qi, et al., "Effect of low levels of sulphate on the current density and film morphology during anodizing of aluminium in chromic acid," *Electrochim. Acta*, **196**, 206 – 222 (2016).
12. H. Zhu, Y. Xu, Y. Han, et al., "Self-powered electrochemical anodic oxidation: A new method for preparation of mesoporous Al_2O_3 without applying electricity," *J. Nano Res.*, **8**(11), 3604 – 3611 (2015).
13. C. K. Chung, M. W. Liao, H. C. Chang, and C. T. Lee, "Effects of temperature and voltage mode on nanoporous anodic aluminum oxide films by one-step anodization," *Thin Solid Films*, **520**(5), 1554 – 1558 (2011).
14. H. Elkilany, A. Hagar, M. Shoeib, et al., "Influence of hard anodizing on the mechanical and corrosion properties of different aluminum alloys," *Metallog. Microstruct. Anal.*, **8**(6), 861 – 870 (2019).
15. M. Sieber, R. Morgenstern, I. Scharf, and T. Lampke, "Effect of nitric and oxalic acid addition on hard anodizing of AlCu4Mg1 in sulphuric acid," *Metals*, **8**(2), 139 (2018).
16. Y. Yang, J. Shen, X. D. Yan, et al., "Effect of alloying elements on the quality of hard anodic oxidation film in aluminum alloy 6061," *Rare Metal Mat. Eng.*, **40**(3), 59 – 62 (2011).
17. R. T. Hitchcock, "Testing of hard anodic-oxidation coatings," *Trans. Inst. Met. Finish.*, **69**, Part 3, 100 – 106 (1991).
18. *ASM Handbook Committee. Metallography and Microstructures ASM Handbook. Vol. 9*, Materials Information Company (2004).
19. *Metallic and Other Inorganic Coatings – Vickers and Knoop Micro-Hardness Tests*, TS 6503 EN-ISO 4516 (2003).
20. *Metallic Materials – Vickers Hardness Test-Part*, Test Method ISO 6507-1 (2018).
21. *ASTM E92. Standard Test Methods for Vickers Hardness and Knoop Hardness of Metallic Materials* (2017).
22. *ASTM G76. Standard Test Methods for Micro-Indentation Hardness of Materials*, ASTM E384 (2017).
23. *ASTM G76. Standard Test Method for Conducting Erosion Tests by Solid Particle Impingement Using Gas Jets*, ASTM International (2018).

24. MIL STD 3033, Department of Defence Particle. Sand Erosion Testing of Rotor Blade Protective Materials, Test Method Standard (2010).
25. A. W. Ruff and L. K. Ives, "Measurement of solid particle velocity in erosive wear," *Wear*, **35**(1), 195 – 199 (1975).
26. TS EN ISO 16610-21. Geometrical product specifications(GPS) — Filtration. Part 21: Linear Profile Filters: Gaussian Filters, International Standards Organization (2013).
27. EN 10049. Measurement of roughness average Ra and peak count R_{Pc} on metallic flat products (German Version), European Standard, Reapproved (2014).
28. TS 6956 EN ISO4287. Geometrical Product Specifications (GPS) — Surface Texture: Profile method — Terms, Definition Sand Surface Texture Parameters, International Standards Organization (2004).
29. T. H. Kosel, *ASM Handbook Committee, Friction, Lubrication and Wear Technology, Solid Particle Erosion*, ASM International (1992), pp. 367 – 396; ASM Handbook, Vol. 18, Electronic version.
30. L. R. Krishna, A. S. Purnima, and G. Sundararajan, "A comparative study of tribological behavior of microarc oxidation and hardanodized coatings," *Wear*, **261**(10), 1095 – 1101 (2006).
31. P. Kwolek, K. Krupa, A. Obłój, et al., "Tribological properties of the oxide coatings produced onto 6061-T6 aluminum alloy in the hard anodizing process," *J. Mater. Eng. Perform.*, **27**(7), 3268 – 3275 (2018).